On the shear resistance and strain-softening sensitivity in the scratch response of a $Cu_{47}Zr_{46}Al_7$ bulk metallic glass

Paul Laffont[a], Marc Fivel[a], Solène Barlemont[b], Pierre-Henry Cornuault[b], Guillaume Colas[b], Alexis Lenain[c], Jean-Jacques Blandin[a], Rémi Daudin[a]*

[a]Grenoble Alpes University, CNRS, Grenoble INP, SIMaP, Grenoble, France

[b]Université Marie et Louis Pasteur, UFR-ST, CNRS, institut FEMTO-ST, F-25000 Besançon, France

[c]Vulkam Inc. Amorphous metal micro casting, Gières 38610, France

*Corresponding author: remi.daudin@simap.grenoble-inp.fr

ABSTRACT

The high mechanical resistance of metallic glasses makes them innovative substitutes for conventional crystalline metals in mechanical and micromechanical applications, but their durability in real system remains difficult to evaluate. Historically, the hardness has been regarded as the most crucial parameter in predicting the wear and the scratch resistance of materials. Metallic glasses are no exception to this convenient but too imprecise rule. It is now generally admitted that additional mechanical parameters, reflecting the structural state, must be taken into account to predict more accurately the robustness of metallic glasses. Using the bonded interface technic, indentation and scratch tests were conducted on a $Cu_{47}Zr_{46}Al_7$ (at.%) metallic glass to evaluate the role of the specific plastic deformation mechanisms of metallic glasses during the formation of a scratch groove. The analysis of shear banding activity below and along the scratch helps to explain the observed morphology of the shear bands and the consequence of associated strain softening on the scratch depth is highlighted. The length of the shear bands below the scratch groove is found to be correlated with the scratch resistance as well as with the length of the shear bands observed on the surface. This offers a useful surface indicator to evaluate scratch resistance without the use of the challenging bonded interface technique for future studies

Keywords: metallic glasses, shear-resistance, strain-softening, scratch response.

Highlights:

- The combination of surface shearing and normal loading causes the deviation of shear-bands below the scratch groove.
- The presence of shear bands ahead the indenter induces strain-softening and the deepening of the scratch groove.
- The scratch depth correlates with shear-band length both below and along the scratch groove.

1. Introduction

The mechanical properties of bulk metallic glasses (BMG) through tensile, compressive, indentation or even bending tests are well documented but their resistance to wear has been less addressed in the literature. However, it is directly linked to the reliability and the durability of the materials. Understanding the deformation mechanisms during diverse, complex and prolonged contacts is of prime importance to improve their integration into real applications.

As metallic glasses exhibit high strength and spatially homogeneous structure, their tribological properties are promising compared to other crystalline alloys [1,2]. It is generally stated that metallic glasses, as other metallic alloys, are in relative good agreement with the Archard's law [3] which states that, in specific contact cases, the wear resistance of a material increases with the increase of its hardness (H) [4]. However, it has also been shown that the original Archard's equation can sometimes be misleading to predict wear loss. For example, modification of this law was proposed to account for the elastic properties of a given material [5] and many questions concerning the impact of others materials properties or contact conditions remain unanswered.

Recent studies using ball-on-plate set-up with reciprocating sliding conditions at low contact pressure have demonstrated that wear mechanisms can evolve in response to changes in surface chemistry [6,7] and/or humidity content [8]. Using ball-on disk test on different metallic glasses, Liao *et al* showed that both hardness and toughness properties are also pivotal factors in determining wear resistance. [9].

Micro-scratch test with a diamond indenter is an appropriate method to evaluate the wear resistance of metallic glasses based on their mechanical properties, while limiting the influence of chemical effects. Recently, Bajpai *et al*. studied the scratch behaviour with a diamond Rockwell indenter of a Zr-based MG thermally treated at different temperatures to reach different energetic states [10]. The findings indicate that, in addition to hardness, fracture toughness can be a significant property, in accordance with the results previously reported by Liao *et al* [9].

Using similar scratch test conditions, Liu *et al*, studied the behaviour of different MG compositions exhibiting different mechanical properties, using progressive normal load [11]. The compositions with the highest hardness values presented both lowest penetration and residual depths, in apparent agreement with the Archard's law. However, the scratch widths do not follow a similar trend. For instance, for the same normal load, the "soft" Ti-based MG (H=4.45 GPa, Knoop hardness) exhibited a scratch width of 50 µm while the "hard" Hf-based MG (H=5.24 GPa, Knoop hardness) exhibited a larger scratch width of 80 µm. In addition, a greater number of cracks was observed along the edge of the scratch groove of the Hf-based MG, compared to the Ti-based MG. These cracks exhibit analogous characteristics than surface shear bands (SB) already observed around or below indentation imprints [12–15] or scratch grooves in other studies [16,17]. As shear bands are the macroscopic features of plastic strain in metallic glasses [18], these observations suggest that plastic deformation mechanisms during scratch should also be taken into account. Indeed, optimising the nucleation and the propagation

of shear bands, was for example found to improve the wear resistance by delaying surface failure of the material [19,20].

On the contrary, despite high hardness values, Ni-based MG were reported to exhibit poor abrasive wear resistance due to very limited plastic properties leading to local failure during scratch test [21]. It therefore suggests that the role of plastic deformation through shear band activity in the scratch resistance of MG must be studied in more details.

To address this lack of knowledge, two major aspects concerning shear banding during the formation of a scratch are studied in the present paper: (i) the shear band activity below and along the scratch groove and (ii) the potential impact on scratch behaviour of local strain-softening linked to the specific heterogeneous plastic deformation of metallic glasses [22].

To do so, scratch tests were performed at the surface of a $Cu_{47}Zr_{46}Al_7$ (at%) metallic glass using in particular the "bonded interface" technique [12,16] (see Materials and Methods). A diamond spherical tip was chosen to allow direct comparisons with recent studies [10,11]. The correlation between the shear band pattern below the scratch groove and at the surface is detailed and the role of deformation induced softening is discussed.

2. Materials and Method

$Cu_{47}Zr_{46}Al_7$ (at.%) ingots of the primary alloy were produced by melting Cu, Zr, and Al metals with ultra-high purity (>99.99%) using an arc melting device under argon and a Ti getter to control the purity of the atmosphere. Each ingot of primary alloy was melted at least five times to ensure good chemical homogeneity. The primary alloy ingots were then melted by induction and injected under controlled atmosphere resulting in plate-shaped samples of 1 x 10 x 15 mm^3.

All the samples were polished using P4000 SiC abrasive papers. X-ray diffraction measurements were performed to ensure the amorphous nature of the structure using a PANanalytical equipment with Cu-Kα radiation. Differential scanning calorimetry measurements were performed using a Mettler Toledo 3+ equipment, under N_2 flux. Samples were heated from room temperature to 973 K at a heating rate of 20 $K.min^{-1}$. The glass transition temperature and the crystallization temperature were extracted at the onset of the transformation and were found to be 696 K and 763 K, respectively.

A Grindosonic MK7 was used to measure the Young's modulus of the produced samples and a value of 90 GPa was found. Vickers' indentation tests were performed using a diamond pyramid indenter with a tip angle of 136°. The instrumented indentation tests were conducted on a MCT3 Anton Paar device at a strain rate of 0.005 s^{-1} up to a maximum load of 30 N which was maintained constant during 20 seconds before unloading, the hardness value was extracted by measuring the contact area with an optical microscope and was found to be of the order of 500 HV, in agreement with previous studies [23,24].

Scratch and indentation tests were performed on the same equipment (Anton Paar MCT3) with a Rockwell indenter with a tip radius of 100 µm and a 120° conical angle, similar to other studies [11]. With this geometry, the indenter can be approximated as a perfect sphere until a limit of the depth of 14.5 µm [11]. During scratch tests, both the penetration depth (P_d) and the

lateral force (F_L) are measured. The friction coefficient (μ) is taken equal to the ratio of the lateral load (F_L) over the applied normal load (F_N) ($\mu = F_L / F_N$).

A first series of scratch tests was carried out using continuous ramp loading from 0 N to 30 N over a length of 4 mm at a speed of 4 mm/min. The results confirmed the necessity to remain below normal load values of 15 N in order to stay in the ploughing regime by avoiding the indenter to go deeper than 14.5 µm into the matter [11], which leads to the formation of chips and too large variations of μ, due to instabilities at the indenter/surface contact.

The second campaign of scratch tests, at the heart of the present study, were also carried out over a total length of 4 mm, at 4 mm/min, but using incremental increases of the normal load to perform 4 successive scratch stages at 2 N, 6 N, 10 N and 14 N, without losing the contact between each stage. This procedure was carried out both on the plain surface of the sample and the commonly called "bonded interface".

The bonded interface was prepared as follows: the sample was cut in two pieces and the edges of both pieces were polished using P4000 SiC abrasive papers and a 1 µm diamond solution to obtain a mirror-like surface. The two pieces were joined back together inside epoxy resin and the top surface was polished a second time using P4000 SiC abrasive papers and then 1 µm diamond to correct a potential height difference between the two pieces. Rockwell indentations were performed at the surface of the sample at the exact location of interface at the following loads: 2, 6, 10 and 14 N using the same tip as the one used for the scratches (R=100 µm / 120°). Scratches with constant loading (2, 6, 10 and 14 N) were also performed along and across the interface. After all indentation tests and scratch tests were performed, the two pieces of the samples were detached. Berkovitch nano-indentation maps composed of 110 indents, separated by 4 µm, were subsequently conducted below the scratch inside the interface using a UNHT3 Anton Paar device.

Images of the different indentation and scratch grooves tracks were made using a Zeiss ultra 55 SEM-FEG operating at 5 kV with a secondary electron detector.

3. Results and discussion

Figure 1 shows the evolution of the averaged penetration depth (Pd) and averaged friction coefficient as a function of the normal load during load jumps test (2 N, 6 N, 10 N and 14 N). The averaging was made over eight different scratches. The raw curves are given in Supplementary Materials, together with the corresponding SEM images (Figure S1 and S2). The penetration depth increases linearly with the load, reaching average values of around 2 µm, 5.5 µm, 7.5 µm and 10.5 µm for 2 N, 6 N, 10 N and 14 N, respectively, with a relatively low standard deviation.

Concerning the friction coefficient, an increase of its average value (0.18, 0.19, 0.21 and 0.23 for 2 N, 6 N, 10 N and 14N, respectively) is also measured for each loading increment. Indeed, as the penetration depth increases, the indenter is surrounded by a greater amount of matter

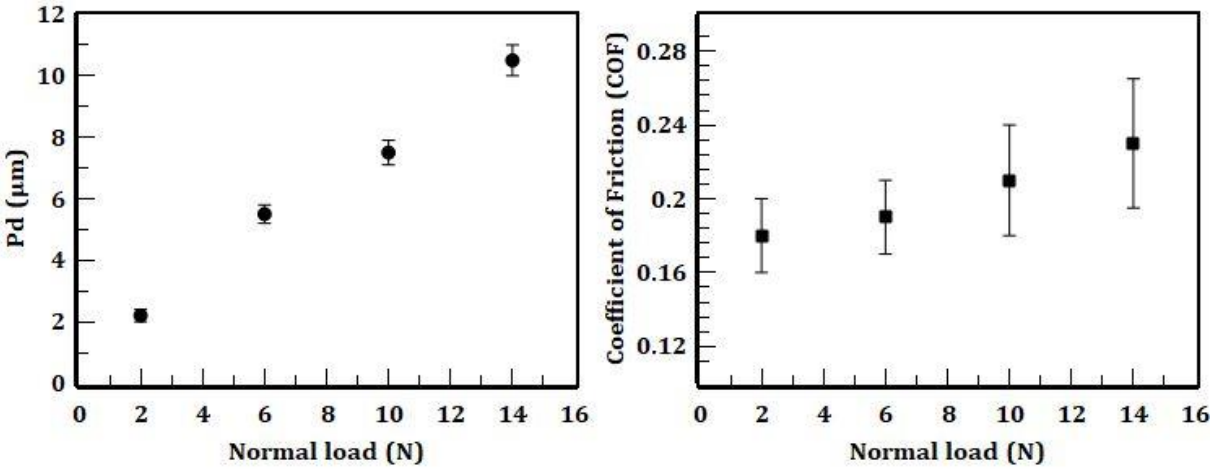

Figure 1 : Averaged penetration depth (Pd) and friction coefficient as a function of the normal load during load jumps scratch tests at 2 N, 6 N, 10 N and 14 N.

which in turn increases the detected lateral load [25]. The standard deviation is relatively large, arising both from the presence of a transitory regime at the beginning of each step and some small differences between the different scratches (see Supplementary Materials). Nevertheless, the average values of the friction coefficient (and the penetration depth) are in very good agreement with those found in the recent study by Liu *et al* who performed scratch tests with similar conditions (same indenter tip, same loads and similar alloys) [11]. It therefore both supports the reliability of the present results and the possibility to compare our results to those of the literature.

Figure 2 presents a scheme of the bonded interface realization and the respective SEM images in the case of the 10N load. It shows the sub-surface features for the spherical indentation (Figure 2(a)) and for the scratch tests performed both perpendicular and parallel to the bonded

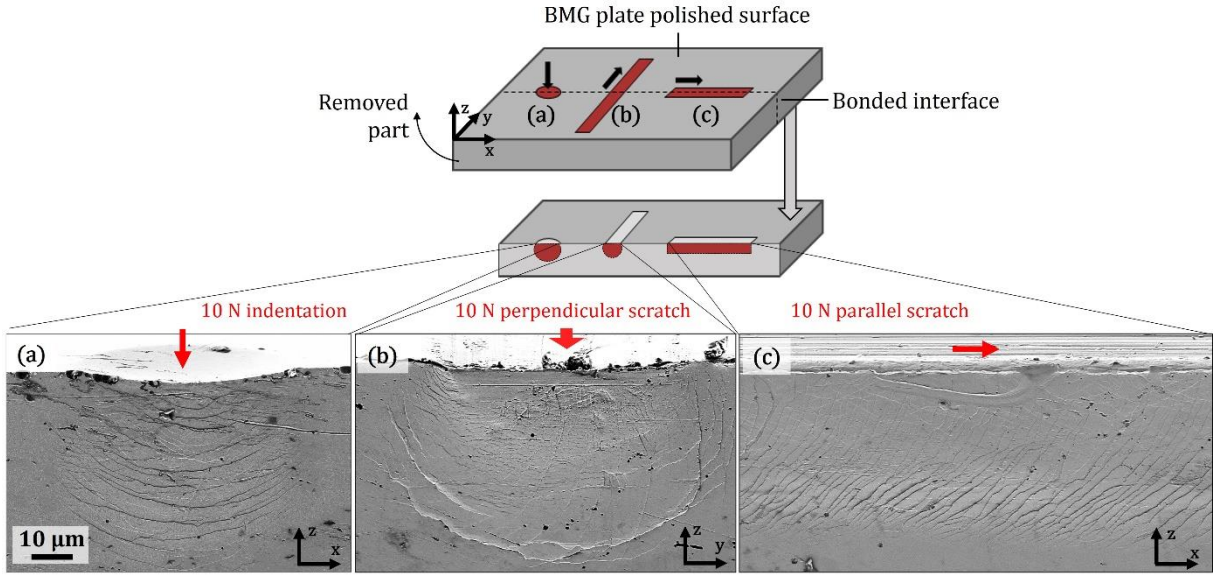

Figure 2: Scheme of the bonded interface preparation and subsequent tests together with respective SEM images at 10 N: (a) indentation (b) scratch in the transverse direction of the bonded interface and (c) scratch in the parallel direction of the bonded interface.

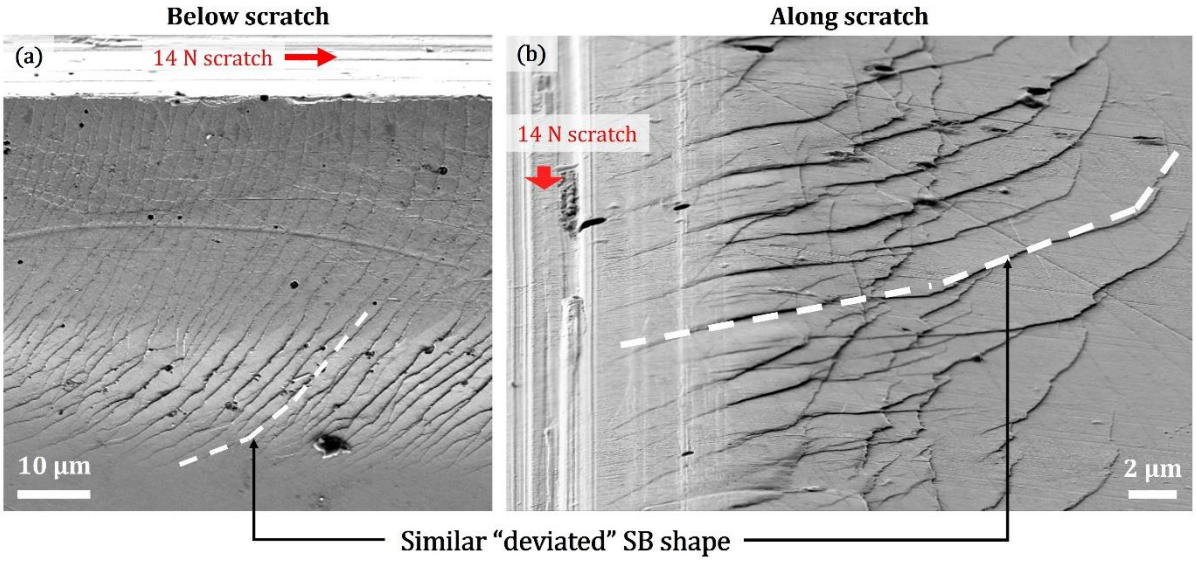

Figure 3 : SEM images of the 14 N scratch (a) in the bonded interface below the scratch and (b) at the surface along the groove.

interface (Figure 2(b) and (c), respectively). The comparison for the other normal load values can be found in the Supplementary Materials (Figure S3, S4, S5). Below the indentation imprint (Figure 2 (a)), convex SB are observed, which is consistent with previous studies [17,26,27]. The characteristic of such network of hemi-spherical SB arises from the stress field induced by the sphero-conical indenter in agreement with the analysis of Packard *et al*. showing that SB formation is controlled by the presence of high stresses along the whole length of a viable shear plane [27]. The fact that the SB do not reach the free surface has also already been observed. It is explained by distribution of the local pressure according to the Hertzian contact theory. It correlates the SB free regions with areas where the local pressure is below a critical value, i.e. the yield stress, to produce SB [15]. As a result, in an indentation test, sufficient stress must be reached, throughout the use of sharp indenters [12,26] and/or the application of important loads [27], for the observation of shear bands at the surface [12,26,27].

Remarkably, below the scratch performed perpendicularly to the bonded interface, only one or two major convex SB are observed, far from the surface (Figure 2(b)). This is a first illustration of the fact that the BMG deformation response to indentation and scratch tests is not similar. The bonded interface in the direction parallel to the scratch direction (Figure 2 (c)), a series of SB that are almost perpendicular to the surface in the vicinity of the scratch groove is observed. They deviate more and more from their original direction and are more branched far from the surface. Figure 3 (a) and (b) highlight the similar characteristic of the SB networks below and at the edge of the scratch groove. At some point, the SBs deviate from their initial propagation direction. Similar observations can be extracted in the perpendicular and parallel views for all normal loads (see Supplementary Materials) showing that the SBs propagate monotonously deeper below the surface with the increase of the normal load, therefore also in correlation with the increase of the penetration depth (see Figure 4). To further understand the origin of this SB pattern arising during scratch tests, it is interesting to focus on the extremity of the scratch groove where the indenter was removed after the last stage at 14 N (Figure 5 (a)). The image

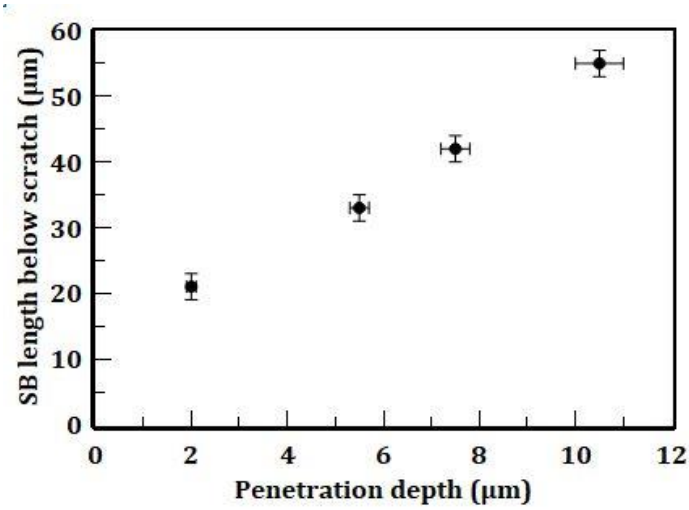

Figure 4 : Shear bands length below scratch as a function of the penetration depth

shows, both on the surface and below the surface: the scratched area, the location where the indenter was stopped and removed as well as the unscratched area. In this latter section ahead of the indenter, some SB can clearly be observed even though no normal load was applied. The length of the SB appears to decrease with the distance from the end of the scratch, the SB at the very right of the image being almost completely vertical and without branching. The presence of such SB can be attributed to the variation of the shear component due to the resistance of the

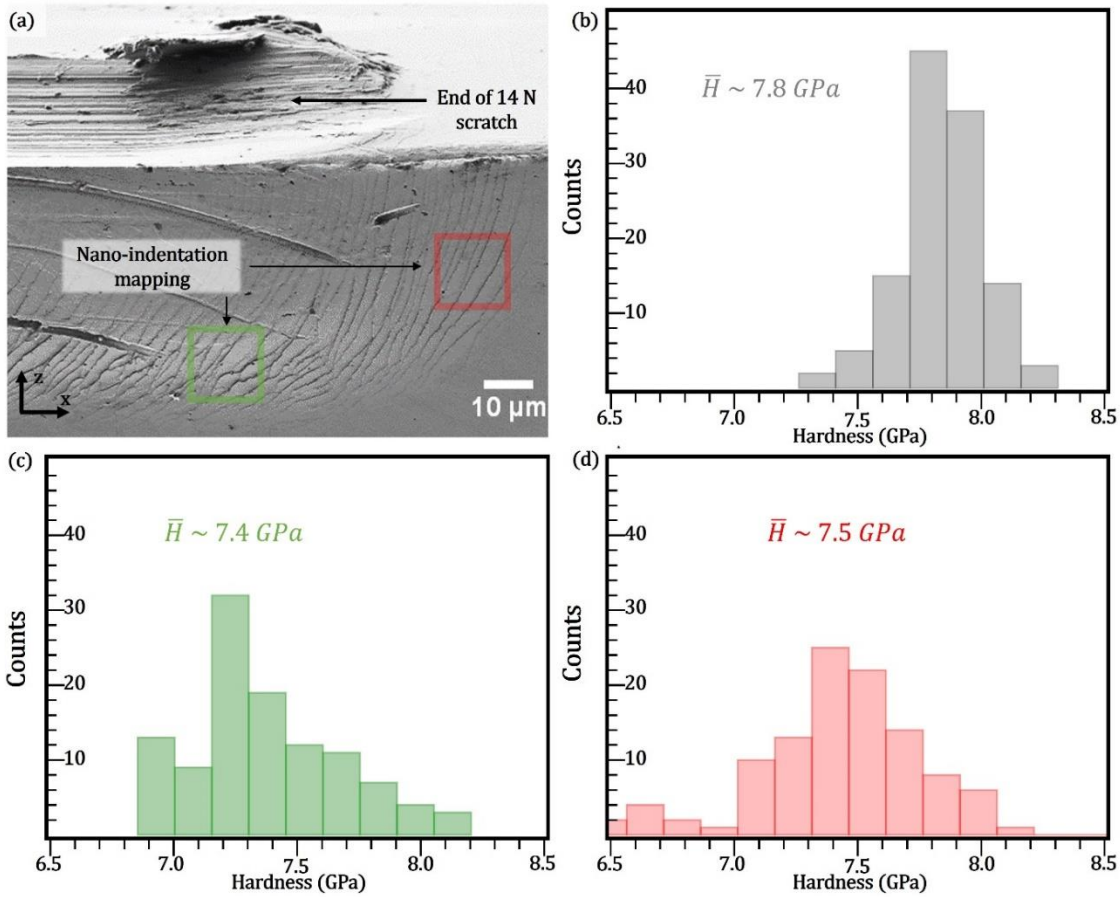

Figure 5 : (a) SEM image of the bonded interface in the longitudinal plane at the end of the 14 N scratch. Green and red squares show where the hardness analysis using nano-indentation with a Berkovitch tip were performed. Hardness values histograms (b) far from scratch (grey), (c) below scratch (green) and (d) in front of the scratch (red).

metallic glass opposed to the motion of the indenter and therefore induced by the tangential force. Indeed, the material subjected to a scratch test experiences a rather complex dynamic stress field. Using Finite Element Method, Jiang *et al* have shown that the matter raised in the pile-up in front of the tip is subjected to tensile conditions which quickly turns into compression conditions below the surface in front of the tip, reaching a maximum right below the tip, and finally switch back to tensile conditions behind the tip [28]. Such stress field arises with the variations of the force direction resulting from the combination of F_N and F_T along the curved surface of the tip and correlates well with the shape of the observed SB. Beneath the front portion of the tip, the resulting force direction is deviated from the vertical direction inducing SB deviated from the 45° direction relative to the vertical (first part of SB below the surface). At the bottom part of the indenter, only F_N is involved and the maximum shear stress direction make the well-known 45° angle with the vertical, resulting in the deviation of SB (second part of SB located at ~40 µm below the surface). Behind the indenter, the tensile conditions may be responsible of more deviation as well as branching of the end of the SB. Such mechanisms, described here with a "three-steps scenario" takes place in reality in a continuous way and result in the progressively curved SB with final branching observed in the bonded interface.

As it is known that the nucleation and the propagation of SB can modify the surrounding metallic glass composition [29,30] and/or structure [31], EDX analyses and nano-indentation investigations were carried out to probe such modifications. Compositional EDX mapping and line analyses across SB were recorded and reveal no detectable chemical segregation (see Fig S6). Nano-indentation tests were performed at different locations at the bonded interface: far from the scratch, below the scratch (green square in Figure 5 (a)) and ahead the end of the scratch (red square in Figure 5 (a)). From the hundred indentation tests performed at each position (see Materials and Methods), the local hardness histograms can be extracted and compared (see Figure 5(b) and (c)). The mean hardness value in the area far from the scratch is 7.84 ± 0.16 GPa while it is 7.37 ± 0.3 GPa and 7.45 ± 0.37 GPa below and in front of the scratch, respectively, showing that the hardness decreases in the regions containing the shear bands with an increase of the standard deviation presumably arising from a more heterogeneous structure in presence of the shear bands.

This result confirms that plastic deformation through shear bands decreases the local mechanical resistance of the material. It is in agreement with numerous studies, both experimental [15,32,33,33–36] and numerical [37–39], showing that strain localisation is correlated to strain softening in metallic glasses. In the specific case of the plastic deformation mechanisms during scratch, Hua *et al* [40,41] used molecular dynamics simulations to study the percolation and the interactions of shear transformation zones (STZ) below the indenter that lead to the formation of shear bands [18]. They highlight that the percolation of STZs is a key mechanism driving strain-softening, as it results in localized plastic flow and the loss of load-bearing capacity of the metallic glass. The introduction of interfaces such as graphene [41] or amorphous/amorphous nanolaminates [40] is proposed to prevent the shear deformation. With these interfaces, the size of the plastic-affected region is found to decrease below the scratch groove and mitigate the softening effect. Here, in the case of a monolithic metallic glass, the

difference in hardness between the two regions containing shear bands seems to be correlated to the number of SB. Indeed, the SB ahead of the indenter are shorter and less branched resulting in a reduction of the strain-softening effect. Consequently, in the present context of scratch resistance, it raises the question to what extent this particular feature taking place in metallic glasses can influence the development of the scratch groove, and therefore the scratch resistance? With this scenario in mind, it implies that compared to a conventional indentation test, the normal load during a scratch test is applied in a material that already contains SB, i.e. in a plastically pre-deformed sample with lower mechanical resistance.

An illustration of the impact of strain softening during scratch can be seen at the transition between two regions performed at different loads, for example in Figure 6 when increasing the load from 6 N to 10 N. On the left-hand side of the image, the indenter scratched the surface with a normal load of 6 N, the corresponding penetration depth is equal to roughly 6 µm and the SB network extends approximately 34 µm below the surface (distance D, white dashed line). At the end of the 6 N stage, the load is quickly increased from 6 N to 10 N with a negligible translation distance resulting in transient indentation test. At this point, the indentation sequence was carried out in the presence of a SB network still extending to 34 µm below the surface. The measured penetration depth increases and reaches 8.3 µm and the remaining SB depth increases to 40 µm. Immediately after this indentation sequence, the scratch test proceeds further. As

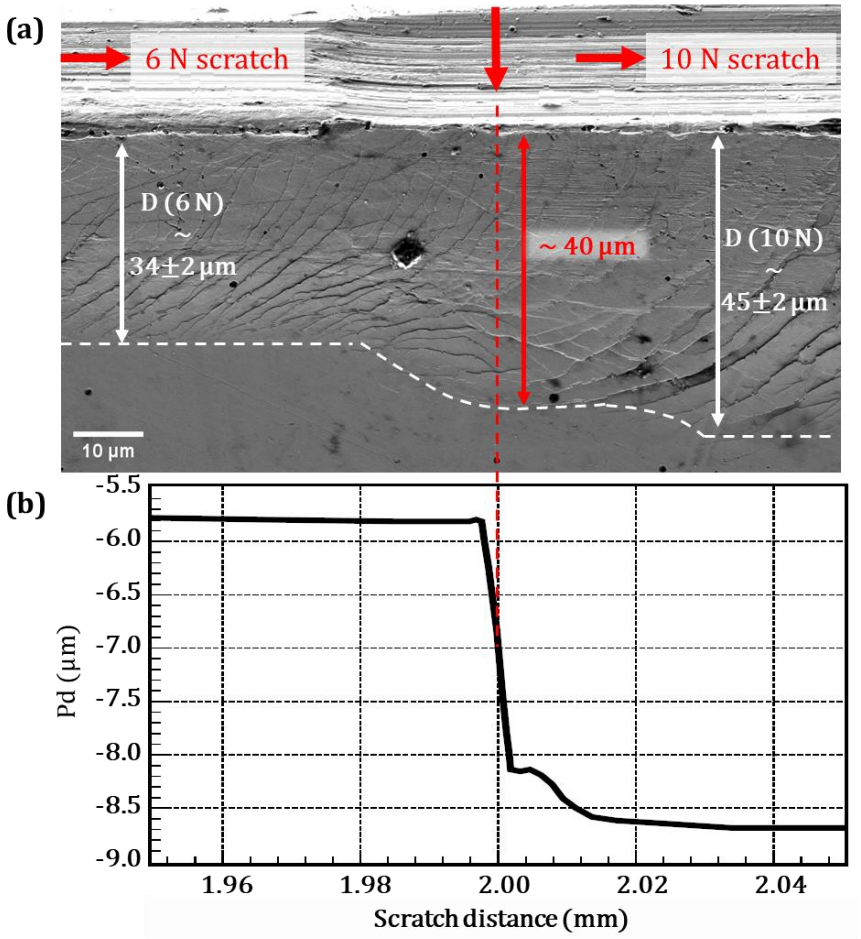

Figure 6 : (a) SEM image of the bonded interface in the parallel plan of the scratch at the transition step of the normal load between 6 N and 14 N (b) Penetration depth (Pd) as a function of the scratch distance.

demonstrated above, the translation of the indenter leads to the creation of the tangential force resulting in the creation of a SB network downstream of the indenter. This part of matter is subjected to strain softening (Figure 5(c)) and therefore offers less resistance. As a consequence, the indenter sinks a little deeper, reaching a stationary penetration depth of 8.9 µm and an increase of the SB depth is observed from 40 µm to roughly 45 µm. The presence of strain softening ahead the indenter due to the SB arising from surface shearing of the matter therefore results in an increase of the penetration depth. Therefore, it can be concluded that there is a correlation between the length of the SB below the scratch and the penetration depth (see Figure 4), and therefore the scratch resistance. Nevertheless, the bonded interface technique presents some practical limitation and, while very useful to get detailed insights below the surface, could also be a potential source of artefact, especially during indentation [13] because of the presence of the cutting surface.

In Figure 3, similarities in the morphology between the SB networks under the scratch groove and at the edges of the scratch on the top surface has already been underlined. It is therefore reasonable to investigate if the length of the SB at the surface are indicative of the length of the SB propagating in the bulk. Figure 7(a) and (b) show how the length of the SB in the bulk and

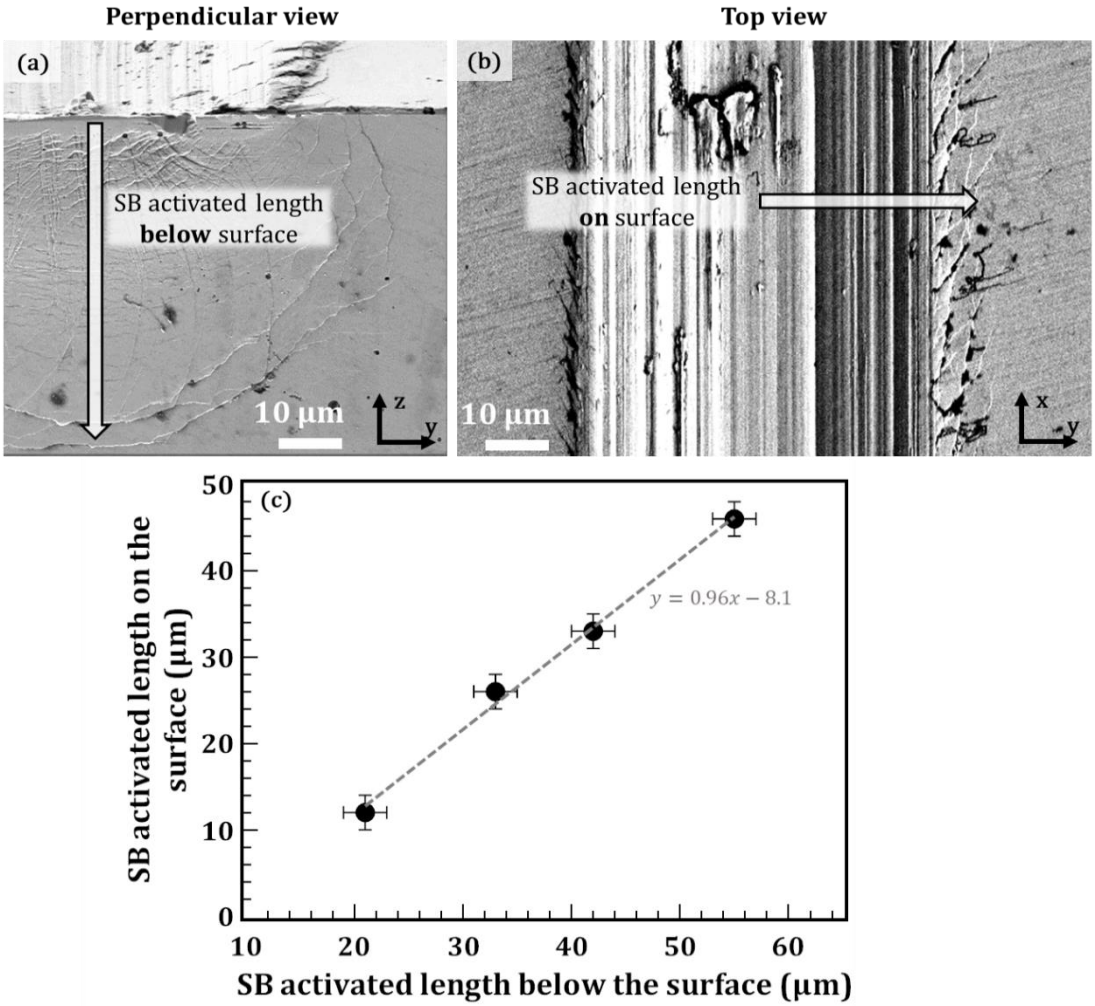

Figure 7 : SEM perpendicular view (a) and top view (b) of a scratch performed at a normal load of 10 N illustrating how the estimated SB lengths were extracted. (c) Correlation between the length of SB below the surface and at the surface.

at the surface were measured. Both lengths are measured on several scratches and for every normal load and the data are plotted in Figure 7(c). It reveals an apparent correlation between the two measurements. This correlation is believed to be important for scratch test analysis of metallic glasses because it provides the possibility of using an easily accessible surface feature to evaluate the length of the SB in the bulk and therefore to estimate the strain-softening impact without necessarily using the bonded interface technic.

The results obtained in the present study emphasize the role played by the pre-existing SB network developing ahead of the indenter tip during scratch tests, which causes strain softening and can therefore modify the scratch resistance. It offers new perspectives to understand more easily some counterintuitive published results (see Introduction section) by taking into consideration the difference in shear resistance, defined as the ratio μ/B between the shear modulus (μ) and the bulk modulus (B). It has been demonstrated that a strong correlation exists between the fracture of metallic glasses and μ/B [42]. Metallic glasses with μ/B > 0.41 are brittle, those with μ/B < 0.32 are tough while those with μ/B between 0.32 and 0.41 abruptly turns from tough to brittle with the increase of μ/B. Table 1 gathers the hardness, Poisson's ratio and μ/B values together with the scratch groove width (W) for two relevant alloys probed using similar conditions by Liu *et al* [11]. The different values for the $Cu_{47}Zr_{46}Al_7$ composition of the present work are also reported for further comparisons.

Composition (at%)	Knoop Hardness (GPa)	Poisson's ratio	μ/B	W (μm, F_N=14 N)
$Hf_{48}Cu_{29.25}Ni_{9.75}Al_{13}$	5.24 [11]	0.349 [43]	0.34	~ 80 [11]
$Ti_{40}Zr_{10}Cu_{38}Pd_{12}$	4.45 [11]	0.369 [44]	0.28	~ 50 [11]
$Cu_{47}Zr_{46}Al_7$	~ 4.25* [11]	0.37 [This work, Supp. Mat.]	0.28	~ 60 [This work, Fig S1]

Table 1 : Knoop hardness, Poisson's ratio, μ/B values and scratch groove width (W, for a normal load of 14 N using diamond Rockwell indenter with 100 μm tips radius). *The Knoop hardness, which cannot be converted from the Vicker's hardness obtained in this work, is taken from [11] for a similar composition ($Zr_{48}Cu_{45}Al_7$) in order to be comparable to the other compositions.

Table 1 shows that a large scratch width, W~80 μm, is measured for the hard Hf-based alloy compared to the softer Ti-based alloy for which a scratch width of only ~50 μm is measured. However, the μ/B values indicates that the Hf-based alloy is also more brittle than the Ti-based. It reveals that, for this specific normal load that may locally induce stresses above the yield stress of the two compositions, the shear-resistance of the metallic glass is of prime importance by mitigating the propagation of SB, delay local final fracture and ultimately reduce the width of the scratch groove. The $Cu_{47}Zr_{46}Al_7$ composition of the present study has the same μ/B value as the Ti-based alloy but a slightly smaller hardness value. The wider measured scratch groove of ~60 μm is therefore consistent: it remains below the width of the hardest but more brittle Hf-based alloy.

It must be pointed out that the shear resistance is also strongly dependent on the structural state (casting conditions, relaxed or rejuvenated state for example) and the later can therefore also

impact the characteristics of the strain-softened volume below the indenter and counter-balance the impact of the hardness. These particular points will be addressed in future studies.

4. Conclusion

In order to probe the relevance of the plastic deformation mechanisms during scratch in metallic glasses, a $Cu_{47}Zr_{46}Al_7$ sample was investigated both by indentation and scratch tests using the bonded interface technique. The main results are listed hereafter:

Load jumps scratch tests resulted in the measurements of friction coefficients ranging from 0.18 to 0.23, in good agreement with previous study with similar metallic glasses and similar tip

The SB pattern below the scratch groove in the bonded interface is « vertical » near the surface, deviated and branched far from the surface. A similar pattern along the edge of the scratch groove at the surface is observed.

This specific SB network pattern originates from the creation of SB ahead of the scratch due to surface shearing arising from the lateral motion of the indenter. When the indenter subsequently applies a normal load on these pre-existing SB, these latter are deviated in the direction parallel to the surface.

The presence of SB, both below and ahead the scratch groove, was found to induce strain softening leading to the increase of the penetration depth and therefore of the scratch dimensions.

The scratch resistance of the studied BMG, evaluated throughout the penetration depth, is correlated with the length of the SB below the scratch groove as the presence of longer SB favours strain-softening of the material.

In addition to the hardness of the metallic glass, the strain softening dependency via shear resistance (μ/B), which depends on the composition but also the structural state, must be taken into account to better evaluate the scratch resistance.

A good correlation between the lengths of the SB observed at the surface and below the surface is measured, which allows the practical possibility to limit the use of “bonded interfaces” in future studies.

Acknowledgments

This work was supported by TRIBORAMA project funded by the French National Research Agency (ANR) (ANR-19-CE08-0015).

Data Availability

Data will be made available on reasonable request.

Author contributions

P.L. : Conceptualization, Data curation, Formal analysis, Investigation, Methodology, Writing – original draft ; **M.F. :** Data curation, Formal analysis, Investigation, Methodology, Supervision, Writing – review and editing ; **S.B. :** Investigation, Methodology, Writing – review and editing; **P-H.C. :** Conceptualization, Formal analysis, Funding acquisition, Investigation, Methodology, Project administration, Resources, Supervision, Writing – review and editing ; **G.C. :** Conceptualization, Formal analysis, Investigation, Methodology, Writing – review and editing ; **A.L. :** Conceptualization, Funding acquisition, Resources ; **J-J.B. :** Conceptualization, Formal analysis, Funding acquisition, Methodology, Project administration, Resources, Supervision, Writing – review and editing ; **R.D. :** Conceptualization, Formal analysis, Funding acquisition, Investigation, Methodology, Project administration, Resources, Supervision, Writing – review and editing.

References

[1] D.C. Hofmann, L.M. Andersen, J. Kolodziejska, S.N. Roberts, J.-P. Borgonia, W.L. Johnson, K.S. Vecchio, A. Kennett, Optimizing Bulk Metallic Glasses for Robust, Highly Wear-Resistant Gears, Advanced Engineering Materials 19 (2017) 1600541. https://doi.org/10.1002/adem.201600541.

[2] O.S. Houghton, L.-Y. Schmitt, U.E. Klotz, M.B. Costa, A.L. Greer, Pd- and Zr-based bulk metallic glasses for jewellery applications: Scratch, wear and tarnish behaviour, Materials Science and Engineering: A 924 (2025) 147791. https://doi.org/10.1016/j.msea.2025.147791.

[3] A.L. Greer, K.L. Rutherford, I.M. Hutchings, Wear resistance of amorphous alloys and related materials, International Materials Reviews 47 (2002) 87–112. https://doi.org/10.1179/095066001225001067.

[4] J.F. Archard, Contact and Rubbing of Flat Surfaces, Journal of Applied Physics 24 (1953) 981–988. https://doi.org/10.1063/1.1721448.

[5] R. Liu, D.Y. Li, Modification of Archard's equation by taking account of elastic/pseudoelastic properties of materials, Wear 251 (2001) 956–964. https://doi.org/10.1016/S0043-1648(01)00711-6.

[6] P.-H. Cornuault, G. Colas, A. Lenain, R. Daudin, S. Gravier, On the diversity of accommodation mechanisms in the tribology of Bulk Metallic Glasses, Tribology International 141 (2020) 105957. https://doi.org/10.1016/j.triboint.2019.105957.

[7] G. Colas, M. del C. Marco de Lucas, L. Imhoff, O. Heintz, R. Daudin, A. Lenain, S. Gravier, P.-H. Cornuault, Tribochemistry dependence of Ni62Nb33Zr5 bulk metallic glass on the Cr content of steel counterparts, Tribology International 198 (2024) 109923. https://doi.org/10.1016/j.triboint.2024.109923.

[8] S. Barlemont, P. Laffont, R. Daudin, A. Lenain, G. Colas, P.-H. Cornuault, Strong dependency of the tribological behavior of CuZr-based bulk metallic glasses on relative humidity in ambient air, Friction 11 (2023) 785–800. https://doi.org/10.1007/s40544-022-0680-z.

[9] Z. Liao, N. Hua, W. Chen, Y. Huang, T. Zhang, Correlations between the wear resistance and properties of bulk metallic glasses, Intermetallics 93 (2018) 290–298. https://doi.org/10.1016/j.intermet.2017.10.008.

[10] S. Bajpai, A. Nisar, R.K. Sharma, U.D. Schwarz, K. Balani, A. Datye, Effect of fictive temperature on tribological properties of Zr44Ti11Cu10Ni10Be25 bulk metallic glasses, Wear 486–487 (2021) 204075. https://doi.org/10.1016/j.wear.2021.204075.

[11] M. Liu, Characterization of bulk metallic glasses by microscratch test under Rockwell C diamond indenter and progressive normal load, Engineering Fracture Mechanics 281 (2023) 109126. https://doi.org/10.1016/j.engfracmech.2023.109126.
[12] V. Keryvin, Indentation of bulk metallic glasses: Relationships between shear bands observed around the prints and hardness, Acta Materialia 55 (2007) 2565–2578. https://doi.org/10.1016/j.actamat.2006.12.005.
[13] V. Keryvin, R. Crosnier, R. Laniel, V.H. Hoang, J.-C. Sanglebœuf, Indentation and scratching mechanisms of a ZrCuAlNi bulk metallic glass, J. Phys. D: Appl. Phys. 41 (2008) 074029. https://doi.org/10.1088/0022-3727/41/7/074029.
[14] S. Xie, E.P. George, Hardness and shear band evolution in bulk metallic glasses after plastic deformation and annealing, Acta Materialia 18 (2008) 5202–5213. https://doi.org/10.1016/j.actamat.2008.07.009.
[15] B.-G. Yoo, J. Jang, A study on the evolution of subsurface deformation in a Zr-based bulk metallic glass during spherical indentation, J. Phys. D: Appl. Phys. 41 (2008) 074017. https://doi.org/10.1088/0022-3727/41/7/074017.
[16] V. Keryvin, X.D. Vu, V.H. Hoang, J. Shen, On the deformation morphology of bulk metallic glasses underneath a Vickers indentation, Journal of Alloys and Compounds 504 (2010) S41–S44. https://doi.org/10.1016/j.jallcom.2010.02.073.
[17] G. Subhash, H. Zhang, Shear Band Patterns in Metallic Glasses under Static Indentation, Dynamic Indentation, and Scratch Processes, Metall and Mat Trans A 38 (2007) 2936–2942. https://doi.org/10.1007/s11661-007-9315-2.
[18] A.L. Greer, Y.Q. Cheng, E. Ma, Shear bands in metallic glasses, Materials Science and Engineering: R: Reports 74 (2013) 71–132. https://doi.org/10.1016/j.mser.2013.04.001.
[19] Q. Zhou, W. Han, Y. Du, H. Wu, A. Bird, X. Zhao, X. Wang, H. Wang, B.D. Beake, Enhancing fatigue wear resistance of a bulk metallic glass via introducing phase separation: A micro-impact test analysis, Wear 436–437 (2019) 203037. https://doi.org/10.1016/j.wear.2019.203037.
[20] Q. Zhou, Y. Du, Y. Ren, W. Kuang, W. Han, H. Wang, P. Huang, F. Wang, J. Wang, Investigation into nanoscratching mechanical performance of metallic glass multilayers with improved nano-tribological properties, Journal of Alloys and Compounds 776 (2019) 447–459. https://doi.org/10.1016/j.jallcom.2018.10.270.
[21] B. Prakash, Abrasive wear behaviour of Fe, Co and Ni based metallic glasses, Wear 258 (2005) 217–224. https://doi.org/10.1016/j.wear.2004.09.010.
[22] H. Bei, Softening Caused by Profuse Shear Banding in a Bulk Metallic Glass, Phys. Rev. Lett. 96 (2006). https://doi.org/10.1103/PhysRevLett.96.105503.
[23] K. Wu, L. Zheng, H. Zhang, Research on high-Al Cu-Zr-Al-Y bulk metallic glass and its composites, Journal of Alloys and Compounds 770 (2019) 1029–1037. https://doi.org/10.1016/j.jallcom.2018.08.130.
[24] R. Wei, X.L. Wang, S. Yang, F. Jiang, L. He, Formation of CuZr-based bulk metallic glass composites containing nanometer-scale B2-CuZr phase through sub- T g annealing, Journal of Alloys and Compounds 617 (2014) 699–706. https://doi.org/10.1016/j.jallcom.2014.08.045.
[25] J. Hong, H. Wu, H. Huang, L. Zhang, Z. Zhang, M. Jiang, J. Yan, The scratch characteristics of laser nitrided Zr-based metallic glass surface, Intermetallics 155 (2023) 107832. https://doi.org/10.1016/j.intermet.2023.107832.
[26] H. Zhang, X. Jing, G. Subhash, L.J. Kecskes, R.J. Dowding, Investigation of shear band evolution in amorphous alloys beneath a Vickers indentation, Acta Materialia 53 (2005) 3849–3859. https://doi.org/10.1016/j.actamat.2005.04.036.

[27] C.E. Packard, C.A. Schuh, Initiation of shear bands near a stress concentration in metallic glass, Acta Materialia 55 (2007) 5348–5358. https://doi.org/10.1016/j.actamat.2007.05.054.
[28] H. Jiang, R. Browning, H.-J. Sue, Understanding of scratch-induced damage mechanisms in polymers, Polymer 50 (2009) 4056–4065. https://doi.org/10.1016/j.polymer.2009.06.061.
[29] E.N. Zanaeva, A.K.A. Lu, D.V. Louzguine-Luzgin, On atomic segregation in metallic glasses induced by shear deformation: A computer simulation study, Computational Materials Science 238 (2024) 112923. https://doi.org/10.1016/j.commatsci.2024.112923.
[30] D.V. Louzguine-Luzgin, A.S. Trifonov, Y.P. Ivanov, A.K.A. Lu, A.V. Lubenchenko, A.L. Greer, Shear-induced chemical segregation in a Fe-based bulk metallic glass at room temperature, Sci Rep 11 (2021) 13650. https://doi.org/10.1038/s41598-021-92907-4.
[31] R. Maaß, K. Samwer, W. Arnold, C.A. Volkert, A single shear band in a metallic glass: Local core and wide soft zone, Applied Physics Letters 105 (2014) 171902. https://doi.org/10.1063/1.4900791.
[32] R. Bhowmick, R. Raghavan, K. Chattopadhyay, U. Ramamurty, Plastic flow softening in a bulk metallic glass, Acta Materialia 54 (2006) 4221–4228. https://doi.org/10.1016/j.actamat.2006.05.011.
[33] I. Binkowski, S. Schlottbom, J. Leuthold, S. Ostendorp, S.V. Divinski, G. Wilde, Sub-micron strain analysis of local stick-slip motion of individual shear bands in a bulk metallic glass, Appl. Phys. Lett. 107 (2015) 221902. https://doi.org/10.1063/1.4936388.
[34] C.-T. Pan, T.-T. Wu, Y.-T. Liu, Y. Yamagata, J.C. Huang, Fabrication of aspheric surface using ultraprecision cutting and BMG molding, Journal of Materials Processing Technology 209 (2009) 5014–5023. https://doi.org/10.1016/j.jmatprotec.2009.01.025.
[35] F.A. Davani, S. Hilke, H. Rösner, D. Geissler, A. Gebert, G. Wilde, On the shear-affected zone of shear bands in bulk metallic glasses, Journal of Alloys and Compounds 837 (2020) 155494. https://doi.org/10.1016/j.jallcom.2020.155494.
[36] M. Zhang, Y. Chen, W. Li, On the origin of softening in the plastic deformation of metallic glasses, International Journal of Plasticity 116 (2019) 24–38. https://doi.org/10.1016/j.ijplas.2018.12.004.
[37] I. Lobzenko, Y. Shiihara, T. Iwashita, T. Egami, Shear Softening in a Metallic Glass: First-Principles Local-Stress Analysis, Phys. Rev. Lett. 124 (2020) 085503. https://doi.org/10.1103/PhysRevLett.124.085503.
[38] Q.-K. Li, M. Li, Atomistic simulations of correlations between volumetric change and shear softening in amorphous metals, Physical Review B 75 (2007). https://doi.org/10.1103/PhysRevB.75.094101.
[39] W. Li, Constitutive Modeling in Metallic Glasses for Predictions and Designs, in: W. Andreoni, S. Yip (Eds.), Handbook of Materials Modeling, Springer International Publishing, Cham, 2018: pp. 1–27. https://doi.org/10.1007/978-3-319-50257-1_103-1.
[40] D. Hua, W. Wang, D. Luo, Q. Zhou, S. Li, J. Shi, M. Fu, H. Wang, Molecular dynamics simulation of the tribological performance of amorphous/amorphous nano-laminates, Journal of Materials Science & Technology 105 (2022) 226–236. https://doi.org/10.1016/j.jmst.2021.07.027.
[41] D. Hua, Q. Zhou, W. Wang, S. Li, X. Liu, H. Wang, Atomic mechanism on the mechanical and tribological performance of amorphous/graphene nanolaminates, Tribology International 165 (2022) 107318. https://doi.org/10.1016/j.triboint.2021.107318.
[42] J.J. Lewandowski *, Wang ,W. H., A.L. and Greer, Intrinsic plasticity or brittleness of metallic glasses, Philosophical Magazine Letters 85 (2005) 77–87. https://doi.org/10.1080/09500830500080474.

[43] L. Zhang, L. Shi, J. Xu, Hf–Cu–Ni–Al bulk metallic glasses: Optimization of glass-forming ability and plasticity, Journal of Non-Crystalline Solids 355 (2009) 1005–1007. https://doi.org/10.1016/j.jnoncrysol.2009.04.009.
[44] J. Fornell, N. Van Steenberge, A. Varea, E. Rossinyol, E. Pellicer, S. Suriñach, M.D. Baró, J. Sort, Enhanced mechanical properties and in vitro corrosion behavior of amorphous and devitrified Ti40Zr10Cu38Pd12 metallic glass, Journal of the Mechanical Behavior of Biomedical Materials 4 (2011) 1709–1717. https://doi.org/10.1016/j.jmbbm.2011.05.028.